

# CONSTRAINING THE BRAKING INDEX AND ENERGY PARTITION OF MAGNETAR SPINDOWN WITH *SWIFT*/XRT DATA

HOU-JUN LÜ, LIN LAN, AND EN-WEI LIANG

Guangxi Key Laboratory for Relativistic Astrophysics, School of Physical Science and Technology, Guangxi University, Nanning 530004, China; lhj@gxu.edu.cn

## ABSTRACT

The long-lasting X-ray plateau emission in long gamma-ray bursts (GRBs) shows observational evidence for ongoing energy injection, which may be from magnetar spindown due to energy released via either magnetic dipole (MD) or gravitational wave (GW) radiation. In this paper, by systematically analyzing the *Swift*/XRT light curves detected before 2018 July, we find 45 light curves with a measured redshift that monotonically decay as a smooth broken power law. By assuming that the central engines of these GRBs are newly born magnetars, we measure the braking index  $n$  of putative millisecond magnetars, due to MD and GW radiations. The inferred braking indices are not close to 3 or 5, but range between them with a normal distribution ( $n_c = 4.02 \pm 0.11$ ). We define a dimensionless parameter  $\mathfrak{R}$ , which is the ratio between the MD and GW components, and find that the energy released via magnetar spindown in most GRBs of our sample is dominated by GW radiation for  $P_0 = 3$  ms and  $\epsilon = 0.005$  and  $0.01$ . On the other hand, we find that  $\mathfrak{R}$  and the braking index  $n$  seem to be anticorrelated within a large systematic error at  $t = 0$ , but depend on the values of the parameters  $P_0$  and  $\epsilon$ . These results suggest that the contribution of GW radiation cannot be ignored, and that a larger braking index leads to GWs dominating the energy released during magnetar spindown if indeed magnetars are operating in some long GRBs.

*Subject headings:* Gamma-ray burst: general

## 1. INTRODUCTION

Millisecond magnetars (namely a rapidly spinning, strongly magnetized neutron stars) are potential candidates for the central engine of gamma-ray bursts (GRBs), which are thought to be from a violent event such as the collapse of a massive star (long GRBs) or the coalescence of two compact objects (short GRBs; Paczynski 1986; Eichler et al. 1989; Usov 1992; Woosley 1993; Thompson 1994; Dai & Lu 1998a,b; MacFadyen & Woosley 1999; Zhang & Mészáros 2001; Metzger et al. 2008; Zhang 2011). Both gravitational wave (GW) and magnetic dipole (MD) radiations can be generated by the rotating neutron star with an asymmetrical mass arrangement (Zhang & Mészáros 2001; Yu et al. 2010; Metzger et al. 2011; Fan et al. 2013; Lasky et al. 2014; Lasky & Glampedakis 2016; Lü et al. 2018). The long-lasting X-ray plateau emission in both long and short GRBs show observational evidence of ongoing energy injection from magnetar spindown (Fan & Xu 2006; Zhang et al. 2006; Liang et al. 2007; Troja et al. 2007; Lyons et al. 2010; Rowlinson et al. 2010; Bucciantini et al. 2012; Rowlinson et al. 2013; Gompertz et al. 2013; Lü & Zhang 2014; Lü et al. 2015; Gao, Zhang & Lü 2016; Chen et al. 2017; Gibson et al. 2017). Unfortunately, the GW signal produced via a rotating neutron star is too weak to be detected by the present-day Advanced LIGO and Advanced Virgo (Abbott et al. 2017; Lü et al. 2017; Sarin et al. 2018).

The energy reservoir of a millisecond magnetar is the total rotation energy, which reads as

$$E_{\text{rot}} = \frac{1}{2} I \Omega^2 \simeq 2 \times 10^{52} \text{ erg } M_{1.4} R_6^2 P_{-3}^{-2}, \quad (1)$$

where  $I$  is the moment of inertia; and  $\Omega$ ,  $P$ ,  $R$ , and  $M$

are the angular frequency, rotating period, radius, and mass of the neutron star, respectively. The convention  $Q = 10^x Q_x$  in cgs units is adopted. A magnetar spinning down loses its rotational energy via MD torques ( $L_{\text{EM}}$ ) and GW ( $L_{\text{GW}}$ ) radiation emissions (Zhang & Mészáros 2001; Fan et al. 2013; Giacomazzo & Perna 2013; Lasky & Glampedakis 2016),

$$\begin{aligned} -\frac{dE_{\text{rot}}}{dt} &= -I\Omega\dot{\Omega} = L_{\text{total}} = L_{\text{EM}} + L_{\text{GW}} \\ &= \frac{B_p^2 R^6 \Omega^4}{6c^3} + \frac{32GI^2 \epsilon^2 \Omega^6}{5c^5}, \quad (2) \end{aligned}$$

where  $B_p$  is the surface magnetic field at the pole and  $\epsilon = 2(I_{xx} - I_{yy})/(I_{xx} + I_{yy})$  is the ellipticity describing how large of the neutron star deformation.  $\dot{\Omega}$  is the time derivative of the angular frequency, and it can be described with the torque equation (Lasky et al. 2017),

$$\dot{\Omega} = -k\Omega^n, \quad (3)$$

where  $k$  is a constant of proportionality, and  $n$  is the braking index<sup>1</sup>.

Traditionally, the physical parameters of magnetars in a GRB study have been estimated by fitting the observed X-ray plateau emission with a magnetar model assuming  $n = 3$  and ignoring the contribution of GW radiation (Troja et al. 2007; Lyons et al. 2010; Rowlinson et al. 2010; Lü & Zhang 2014; Lü et al. 2015). In principle, the contribution of GW radiation to a rotating neutron star should be considered, and the braking index should not be a constant (Fan et al. 2013; Lasky & Glampedakis

<sup>1</sup> Here, we assume that the value of  $k$  is constant, even though it sometimes evolves with time and depends on the equation of state of the neutron star (Woan et al. 2018).

2016). If this were the case, the accurate estimated value of the braking index becomes very important in understanding the properties of the magnetar and the fraction of energy released as GW and MD radiations (Woan et al. 2018). Lasky et al. (2017) first proposed constraining the braking indices of magnetars by invoking the X-ray plateau emission of two short GRBs with measured redshifts. However, they used the observed X-ray plateau luminosity, which is equal to the total luminosity ( $L_{\text{total}}$ ) of the released magnetar energy, to fit the data. In fact, the intrinsic luminosity of GW radiation should not be accounted for when fitting the observed data, although it can affect electromagnetic (EM) emission when GW radiation is dominant in or contributes to the spindown of magnetars. In other words, the  $\Omega(t)$  does not evolve with time, neither following  $\sim t^{-1/2}$  (MD-dominated) nor  $\sim t^{-1/4}$  (GW-dominated) when the time is much longer than the characteristic spindown timescale (Lü et al. 2018).

In this paper, by considering the contribution of GW radiation to magnetar spindown, we perform a systematic study of long GRBs, in whose central engine may reside a millisecond magnetar, and investigate constraining the braking index using the X-ray light curves exhibited by the plateau following normal decay emissions of long GRBs. We also try to determine the fraction of energy released by the magnetar as MD and GW radiations if the magnetar is indeed the central engine of those long GRBs.

This paper is organized as follows. Our sample selection and data for the magnetar model fitting are presented in section 2. The result of braking index constraint of magnetar is shown in section 2. In section 3, we roughly calculate the fraction of magnetar energy released as MD and GW radiations. The conclusions, along with some discussions, are presented in Section 4. Throughout this paper, a concordance cosmology with parameters  $H_0 = 71 \text{ km s}^{-1} \text{ Mpc}^{-1}$ ,  $\Omega_M = 0.30$ , and  $\Omega_\Lambda = 0.70$  is adopted.

## 2. SAMPLE SELECTION AND DATA FITTING WITH THE MAGNETAR MODEL

### 2.1. Sample Selection

Our entire sample includes more than 1300 GRBs observed between 2005 January and 2018 July, the X-Ray Telescope (XRT) data of which were selected and downloaded from the *Swift* data archive and the UK *Swift* Science Data Center<sup>2</sup> (Evans et al. 2010). The magnetar signature typically exhibits a shallow decay phase (or plateau) followed by a steeper decay segment (a normal decay for canonical light curves or a very steep decay for internal plateaus) when it is spinning down by losing rotational energy via MD and GW radiations.

Three criteria are adopted for our sample selection. First, we focus on those long GRBs that show such a transition in the X-ray light curves, but required that the decay slope of the steeper decay segment following the plateau phase should be in range of -1 to -2. Those are the typical decay slopes when GW and MD radiations are dominant, respectively<sup>3</sup> (Zhang & Mészáros 2001; Lasky

& Glampedakis 2016; Lü et al. 2018). Second, GRBs with bright X-ray flares<sup>4</sup> observed during the plateau or normal decay phase are excluded from our sample. Those flares are believed to be from later activity of the central engine (Zhang et al. 2007; Peng et al. 2014). Third, in order to estimate the intrinsic luminosity of the plateau emission, the redshift for our sample needs to be measured. By adopting these criteria for our sample selection, 45 long GRBs are included in our sample (also see Zou et al. 2018). Moreover, GRB 060614 is not included in our sample because its properties satisfy the above criteria, a possible kilonova signature in the near-infrared band points to a compact binary merger origin (Yang et al. 2015).

### 2.2. Data Fitting with the Magnetar Model

As a neutron star forms when a massive star collapses, its angular frequency evolves with time. The solution of Eq.(3) can be expressed as

$$\Omega(t) = \Omega_0 \left(1 + \frac{t}{\tau}\right)^{\frac{1}{1-n}}, \quad (4)$$

where  $\Omega_0$  is the initial angular frequency at  $t = 0$ , and  $\tau = \frac{\Omega_0^{1-n}}{(n-1)k}$  is the spindown timescale of the magnetar. The observed luminosity should be equivalent to  $L_{\text{EM}}$ , namely

$$\begin{aligned} L_{\text{obs}} = L_{\text{EM}} &= \frac{B_p^2 R^6 \Omega^4}{6c^3} \\ &= L_0 \left(1 + \frac{t}{\tau}\right)^{\frac{4}{1-n}} \end{aligned} \quad (5)$$

where  $L_0 = \frac{B_p^2 R^6 \Omega_0^4}{6c^3}$  is the spindown luminosity of the magnetar.

The observed plateau luminosity of the X-ray emission ( $L_X$ ), which is calculated in the (0.3-10)keV energy band by assuming 10% radiation efficiency, is equivalent to  $L_{\text{obs}}$ . Thus, Equation (5) shows the plateau luminosity  $L_X \approx L_0$  for  $t \ll \tau$ , and a power-law decay  $L_X \propto t^{\frac{4}{1-n}}$  for later times  $t \gg \tau$ . It is worth noting that Eq. (5) recovers the evolution of the luminosity with dominant MD radiation for  $n = 3$ , and the spindown timescale becomes the MD-dominated spindown timescale ( $\tau = \tau_{\text{em}}$ ). By the same token, for  $n = 5$ , the luminosity evolution is consistent with GW radiation dominating the magnetar spindown, and  $\tau = \tau_{\text{gw}}$  in this limit (Zhang & Mészáros 2001; Lasky & Glampedakis 2016; Lü et al. 2018; Sarin et al. 2018). Therefore, we adopt Eq. (5) and combine it with an initial power-law decay  $L_X = At^{-\alpha}$  to fit the X-ray light curves of our sample. By fitting the X-ray data, one can obtain the parameters of the magnetar model and the power-law component (e.g.,  $A$ ,  $\alpha$ ,  $L_0$ ,  $\tau$ , and  $n$ ). An example of the light-curve fitting is shown in Fig.1, and other samples are shown in this link: <http://astro.gxu.edu.cn/info/1067/1530.htm>. The fitting results are presented in Table 1.

## 3. RESULTS

<sup>4</sup> Bright X-ray flares are defined as  $F_p/F_b > 5$ , where  $F_p$  and  $F_b$  are the flux at the peak time and the corresponding underlying flux, respectively (Hu et al. 2014; Zou et al. 2018).

<sup>2</sup> [http://www.swift.ac.uk/burst\\_analyser/](http://www.swift.ac.uk/burst_analyser/)

<sup>3</sup> The magnetar may be unstable and collapse into the black hole before it spins down if the decay slope is steeper than 2.

Our purpose is to find out the variable braking index of a magnetar in our sample and the energy partition of a magnetar between GW and MD radiations by using *Swift*/XRT data of long GRBs.

### 3.1. The braking index of magnetars

The top panel of Fig. 1 shows the XRT data, together with our fit using Eq.5 and an initial power law that fits the steep decay phase (dashed-dotted lines). The solid red curve shows the superposition of the magnetar model and power-law fits.

Fig. 2 shows the distribution of the braking indices of the magnetars in our sample. Interestingly, we find that the braking indices are neither close to 3 nor 5, but range between these two values. It is likely a normal distribution with the center value  $n_c = 4.02 \pm 0.11$ . On the other hand, we compare the braking index of our sample with that of all known pulsars in which the long-term spindown is believed to be electromagnetically dominated (Antonopoulou et al. 2015; Archibald et al. 2016; Clark et al. 2016). From the statistical point of view, the distribution of braking indices of our sample is much larger than the distribution of pulsar braking indices, and it indicates that the millisecond magnetar in our sample is intrinsically different from that in normal pulsar. However, due to the limited data, this difference also seems to be caused by a selection effect. To determine whether the distribution of braking indices of our sample is statistically consistent with the distribution of pulsar braking indices, more observational data in the future is needed.

### 3.2. The fraction of magnetar energy released via GW and MD radiations

The braking index of a magnetar is reflected in the behavior of the energy released. With  $n = 3$ , the neutron star is spun down only via a dipole magnetic field in vacuum, while  $n = 5$  implies that the neutron star is spun down through GW radiation (Lasky & Glampedakis 2016; Lü et al. 2018). However, the fraction of energy released by the magnetar as MD and GW radiations when the value of  $n$  in the range of 3-5 remains an open question. In this section, we investigate the evolution with time of the fraction of energy released during magnetar spindown.

Here, we quantify the fraction of energy released by the magnetar by defining the ratio parameter  $\mathfrak{R}$ ,

$$\begin{aligned} \mathfrak{R} &= \frac{L_{\text{EM}}}{L_{\text{GW}}} = \frac{B_p^2 R^6 \Omega^4}{6c^3} \cdot \frac{5c^5}{32GI^2 \epsilon^2 \Omega^6} \\ &= \frac{125}{8192} \cdot \frac{L_0 c^5}{\pi^6 GM^2 \epsilon^2 R^4} \cdot P_{0,-3}^6 \cdot \left(1 + \frac{t}{\tau}\right)^{\frac{2}{n-1}} \quad (6) \end{aligned}$$

where  $L_0$ ,  $\tau$ , and the braking index  $n$  are measured by fitting the X-ray data of long GRBs with the magnetar model. The radius and mass of the neutron star depends on the equation of state.  $\mathfrak{R} \gg 1$  implies that the spindown of the magnetar is dominated by MD radiation, while  $\mathfrak{R} \ll 1$  implies that the magnetar is spun down through GW radiation. The energy released during magnetar spindown is contributed by both MD and GW radiations when  $\mathfrak{R}$  is close to 1. The bottom panel of Fig. 1 shows  $\mathfrak{R} = \frac{L_{\text{EM}}}{L_{\text{GW}}}$  as a function of time by as-

suming  $P_0 = 3$  ms and  $\epsilon = 0.01$  and 0.005 with equation of state GM1 (Lasky et al. 2014; Lü et al. 2018).

Given the initial parameters  $P_0 = 3$  ms and  $\epsilon = 0.005$  and 0.01, the distributions of  $\mathfrak{R}$  tend to normal with center values  $0.47 \pm 0.09$  and  $0.12 \pm 0.04$ , respectively. It suggests that a large fraction of GRBs in our sample with energy released during magnetar spindown are dominated by GW radiation for larger  $\epsilon$  values. Such type of magnetar was also applied in some short GRBs to constrain the ellipticity (Fan et al. 2013; Lasky & Glampedakis 2016).

On the other hand, we investigate how the initial ratio parameter between  $L_{\text{EM}}$  and  $L_{\text{GW}}$ ,  $\mathfrak{R}$ , is related to the braking index  $n$ . Figure 3 presents the  $\mathfrak{R} - n$  correlation at  $t = 0$  for given  $P_0 = 3$  ms by assuming  $\epsilon = 0.01$  and  $\epsilon = 0.005$ , respectively. There seems to be an anticorrelation between  $\mathfrak{R}$  and  $n$ , namely a higher braking index corresponds to a lower  $\mathfrak{R}$  value within a large systematic error. If this anticorrelation indeed exists, it indicates that a higher braking index tends to give rise to GW-dominated radiation for magnetar spindown, and that is consistent with the theoretical derivation in Zhang & Mészáros (2001). However, the derived  $\mathfrak{R}$  value depends on the equation of state, initial period  $P_0$ , and ellipticity  $\epsilon$ , which may be constrained by detecting GW radiation and its associated EM emission simultaneously (Lasky et al. 2014; Li et al. 2016; Lü et al. 2018).

## 4. CONCLUSIONS AND DISCUSSION

The observed X-ray plateau following a steep decay emission in the X-ray light curves of long GRBs is believed to be from the ongoing energy injection of a magnetar and its spindown. In this paper, we systematically analyzed the X-ray light curves of long GRBs detected by *Swift*/XRT before 2018 July. There are 45 long GRBs with redshifts measured whose X-ray light curves exhibited a plateau following a steep decay emission. By assuming that the central engines of these GRBs are newly born magnetars, we measure the braking index  $n$  of the putative millisecond magnetars via the observed X-ray emission with MD and GW radiations. We define a dimensionless parameter  $\mathfrak{R}$  that indicates the fraction of energy released as MD and GW radiations and try to find out the distribution of  $\mathfrak{R}$  initially and its relation with the braking index  $n$ . The following interesting results are obtained.

- The inferred braking indices of the magnetars in our sample are neither close to 3 (i.e., for magnetar spindown dominated by MD radiation) nor to 5 (i.e., for magnetar spindown dominated by GW radiation), but range between them. We find that the distribution of braking indices is likely normal with the center value  $n_c = 4.02 \pm 0.11$ . That value is much larger than that for the distribution of known pulsars, where the long-term spindown is believed to be electromagnetically dominated. It indicated that the energy released by the millisecond magnetars in our sample is intrinsically different from those released by normal pulsars if this difference is not from a selection effect.
- The distribution of  $\mathfrak{R}$  tends to normal with center values  $0.47 \pm 0.09$  and  $0.12 \pm 0.04$  for  $P_0 = 3$  ms

and  $\epsilon = 0.005$  and  $0.01$ , respectively. It indicates that for a small fraction of GRBs in our sample, the energy loss during magnetar spindown seems to be MD-dominated.

- The ratio parameter  $\mathfrak{R}$  and braking index  $n$  seem to be anticorrelated within a large systematic error at  $t = 0$ , although it depends on the values of parameters  $P_0$  and  $\epsilon$ . It suggests that a larger braking index leads to GW dominating the energy released during magnetar spindown.

The braking indices of most long GRBs in our sample range from 3 up to 5, but a small fraction of long GRBs fall out of this range. Several possible models discussed in the literature are invoked to explain the observed anomalous  $n < 3$  braking indices. For example, a twisted magnetosphere consisting of a strong mixed poloidal-toroidal field increases the spindown torque in comparison to orthogonal vacuum dipoles (Thompson et al. 2002; Kiuchi et al. 2011; Turolla et al. 2015), or a different magnetosphere that is dipole force-/twist-free is used (Contopoulos & Spitkovsky 2006). Another possible explanation for  $< 3$  braking indices is related to the evolution of the included angle, which is the angle between the spin axis and its surface dipole magnetic field axis (Lyne et al. 2013; 2015), or to the momentum loss during a neutron star spindown due to both dipole radiation and a episodic or continuous particle winds (Harding et al. 1999).

In comparison to the possible explanations for  $n <$

3 braking indices, there are fewer proposed models for interpreting the  $n > 5$  braking indices. For example, if the magnetar spindown is through unstable  $r$  modes, then the braking index can be as large as 7 (Owen et al. 1998). However, the braking index of a magnetar for unstable  $r$  modes is also insensitive to both microscopic details and the saturation amplitude. If this is the case, the true value of the braking index can be in range of 5-7 (Alford & Schwenzer 2014, 2015). On the other hand, the ratio parameter  $\mathfrak{R}$  depends on the initial period and ellipticity of the magnetar in our calculations, and the true value of  $\mathfrak{R}$  can be constrained if the initial period of the ellipticity can be measured by using independent methods in the future.

We acknowledge the use of the public data from the *Swift* data archive and the UK *Swift* Science Data Center. This work is supported by the National Basic Research Program (973 Programme) of China 2014CB845800, the National Natural Science Foundation of China (grant Nos.11603006, 11533003 and 11851304), Guangxi Science Foundation (grant Nos. 2017GXNSFFA198008, 2016GXNSFCB380005 and 2017AD22006), the One-Hundred-Talents Program of Guangxi colleges, the high level innovation team and outstanding scholar program in Guangxi colleges, Scientific Research Foundation of Guangxi University (grant no XGZ150299), and special funding for Guangxi distinguished professors (Bagui Yingcai & Bagui Xuezhe).

#### REFERENCES

- Abbott, B. P., Abbott, R., Abbott, T. D., et al. 2017, *Physical Review Letters*, 119, 161101
- Alford, M. G., & Schwenzer, K. 2015, *MNRAS*, 446, 3631
- Alford, M. G., & Schwenzer, K. 2014, *ApJ*, 781, 26
- Antonopoulou, D., Weltevrede, P., Espinoza, C. M., et al. 2015, *MNRAS*, 447, 3924
- Archibald, R. F., Gotthelf, E. V., Ferdman, R. D., et al. 2016, *ApJ*, 819, L16
- Bloom, J. S., Perley, D. A., & Chen, H. W. 2006, *GRB Coordinates Network*, 5826, 1
- Bucciantini, N., Metzger, B. D., Thompson, T. A., & Quataert, E. 2012, *MNRAS*, 419, 1537
- Castro-Tirado, A. J., Amado, P., Negueruela, I., et al. 2006, *GRB Coordinates Network*, 5218, 1
- Castro-Tirado, A. J., Cunniffe, R., Sanchez-Ramirez, R., et al. 2014, *GRB Coordinates Network, Circular Service*, No. 16505, #1 (2014), 16505, 1
- Cenko, S. B., Perley, D. A., Jankkarinen, V., et al. 2009, *GRB Coordinates Network*, 9518, 1
- Chen, H.-W., Helsby, J., Shectman, S., Thompson, I., & Crane, J. 2009, *GRB Coordinates Network, Circular Service*, No. 1038, #1 (2009), 10038, 1
- Chen, W., Xie, W., Lei, W.-H., et al. 2017, *ApJ*, 849, 119
- Chornock, R., Cucchiara, A., Fox, D., & Berger, E. 2010, *GRB Coordinates Network, Circular Service*, No. 10466, #1 (2010), 10466, 1
- Chornock, R., Perley, D. A., & Cobb, B. E. 2009, *GRB Coordinates Network, Circular Service*, No. 10100, #1 (2009), 10100, 1
- Clark, C. J., Pletsch, H. J., Wu, J., et al. 2016, *ApJ*, 832, L15
- Contopoulos, I., & Spitkovsky, A. 2006, *ApJ*, 643, 1139
- Cucchiara, A., & Fox, D. B. 2008, *GRB Coordinates Network*, 7654, 1
- Dai, Z. G., & Lu, T. 1998, *Physical Review Letters*, 81, 4301
- Dai, Z. G., & Lu, T. 1998, *A&A*, 333, L87
- de Ugarte Postigo, A., Fynbo, J. P. U., Jakobsson, P., et al. 2011, *GRB Coordinates Network, Circular Service*, No. 12258, #1 (2011), 12258, 1
- de Ugarte Postigo, A., Gorosabel, J., Malesani, D., Fynbo, J. P. U., & Levan, A. J. 2009, *GRB Coordinates Network*, 9381, 1
- de Ugarte Postigo, A., Izzo, L., Kann, D. A., et al. 2017, *GRB Coordinates Network, Circular Service*, No. 22272, #1 (2017), 22272, 1
- de Ugarte Postigo, A., Kann, D. A., Izzo, L., & Thoene, C. C. 2017, *GRB Coordinates Network, Circular Service*, No. 21298, #1 (2017), 21298, 1
- Dittmann, J., Laskar, T., & Berger, E. 2011, *GRB Coordinates Network, Circular Service*, No. 12759, #1 (2011), 12759, 1
- Eichler, D., Livio, M., Piran, T., & Schramm, D. N. 1989, *Nature*, 340, 126
- Evans, P. A., Willingale, R., Osborne, J. P., et al. 2010, *A&A*, 519, A102
- Fan, Y.-Z., Wu, X.-F., & Wei, D.-M. 2013, *Phys. Rev. D*, 88, 067304
- Fan, Y.-Z., & Xu, D. 2006, *MNRAS*, 372, L19
- Fynbo, J. P. U., Hjorth, J., Jensen, B. L., et al. 2005, *GRB Coordinates Network*, 3136, 1
- Gao, H., Zhang, B., & Lü, H.-J. 2016, *Phys. Rev. D*, 93, 044065
- Giacomazzo, B., & Perna, R. 2013, *ApJ*, 771, L26
- Gibson, S. L., Wynn, G. A., Gompertz, B. P., & O'Brien, P. T. 2017, *MNRAS*, 470, 4925
- Gompertz, B. P., O'Brien, P. T., Wynn, G. A., & Rowlinson, A. 2013, *MNRAS*, 431, 1745
- Harding, A. K., Contopoulos, I., & Kazanas, D. 1999, *ApJ*, 525, L125
- Heintz, K. E., Fynbo, J. P. U., & Malesani, D. 2018, *GRB Coordinates Network, Circular Service*, No. 22535, #1 (2018/March-0), 22535, 1
- Hjorth, J., Malesani, D., Jakobsson, P., et al. 2012, *ApJ*, 756, 187
- Hu, Y.-D., Liang, E.-W., Xi, S.-Q., et al. 2014, *ApJ*, 789, 145

- Izzo, L., Heintz, K. E., Malesani, D., et al. 2018, GRB Coordinates Network, Circular Service, No. 22567, #1 (2018/March-0), 22567, 1
- Jakobsson, P., Fynbo, J. P. U., Andersen, M. I., et al. 2007, GRB Coordinates Network, 6398, 1
- Jakobsson, P., Vreeswijk, P., Fynbo, J. P. U., et al. 2006, GRB Coordinates Network, 5320, 1
- Jaunsen, A. O., Thoene, C. C., Fynbo, J. P. U., Hjorth, J., & Vreeswijk, P. 2007, GRB Coordinates Network, 6202, 1
- Kiuchi, K., Yoshida, S., & Shibata, M. 2011, *A&A*, 532, A30
- Krühler, T., Malesani, D., Fynbo, J. P. U., et al. 2015, *A&A*, 581, A125
- Krühler, T., Malesani, D., Milvang-Jensen, B., et al. 2012, *ApJ*, 758, 46
- Kruehler, T., Malesani, D., de Ugarte Postigo, A., Melandri, A., & Fynbo, J. P. U. 2014, GRB Coordinates Network, Circular Service, No. 16194, #1 (2014), 16194, 1
- Kruehler, T., Malesani, D., Xu, D., et al. 2013, GRB Coordinates Network, Circular Service, No. 14264, #1 (2013), 14264, 1
- Lü, H.-J., & Zhang, B. 2014, *ApJ*, 785, 74
- Lü, H.-J., Zhang, B., Lei, W.-H., Li, Y., & Lasky, P. D. 2015, *ApJ*, 805, 89
- Lü, H.-J., Zhang, H.-M., Zhong, S.-Q., et al. 2017, *ApJ*, 835, 181
- Lü, H.-J., Zou, L., Lan, L., & Liang, E.-W. 2018, *MNRAS*, 480, 4402
- Lasky, P. D., & Glampedakis, K. 2016, *MNRAS*, 458, 1660
- Lasky, P. D., Haskell, B., Ravi, V., Howell, E. J., & Coward, D. M. 2014, *Phys. Rev. D*, 89, 047302
- Lasky, P. D., Leris, C., Rowlinson, A., & Glampedakis, K. 2017, *ApJ*, 843, L1
- Li, A., Zhang, B., Zhang, N.-B., et al. 2016, *Phys. Rev. D*, 94, 083010
- Liang, E.-W., Zhang, B.-B., & Zhang, B. 2007, *ApJ*, 670, 565
- Lyne, A. G., Jordan, C. A., Graham-Smith, F., et al. 2015, *MNRAS*, 446, 857
- Lyne, A., Graham-Smith, F., Weltevrede, P., et al. 2013, *Science*, 342, 598
- Lyons, N., O'Brien, P. T., Zhang, B., et al. 2010, *MNRAS*, 402, 705
- MacFadyen, A. I., & Woosley, S. E. 1999, *ApJ*, 524, 262
- Malesani, D., Fynbo, J. P. U., D'Elia, V., et al. 2009, GRB Coordinates Network, 9457, 1
- Malesani, D., Kruehler, T., Heintz, K. E., & Fynbo, J. P. U. 2016, GRB Coordinates Network, Circular Service, No. 20180, #1 (2016), 20180, 1
- Metzger, B. D., Giannios, D., Thompson, T. A., Bucciantini, N., & Quataert, E. 2011, *MNRAS*, 413, 2031
- Metzger, B. D., Quataert, E., & Thompson, T. A. 2008, *MNRAS*, 385, 1455
- O'Meara, J., Chen, H.-W., & Prochaska, J. X. 2010, GRB Coordinates Network, Circular Service, No. 11089, #1 (2010), 11089, 1
- Owen, B. J., Lindblom, L., Cutler, C., et al. 1998, *Phys. Rev. D*, 58, 084020
- Paczynski, B. 1986, *ApJ*, 308, L43
- Peng, F.-K., Liang, E.-W., Wang, X.-Y., et al. 2014, *ApJ*, 795, 155
- Perley, D. A., Krühler, T., Schulze, S., et al. 2016, *ApJ*, 817, 7
- Perley, D. A., Levan, A. J., Tanvir, N. R., et al. 2013, *ApJ*, 778, 128
- Peterson, B. A., & Schmidt, B. 2006, *IAU Joint Discussion*, 1, 42
- Rowlinson, A., O'Brien, P. T., Metzger, B. D., Tanvir, N. R., & Levan, A. J. 2013, *MNRAS*, 430, 1061
- Rowlinson, A., O'Brien, P. T., Tanvir, N. R., et al. 2010, *MNRAS*, 409, 531
- Ruffini, R., Bianco, C. L., Enderli, M., et al. 2013, GRB Coordinates Network, Circular Service, No. 14888, #1 (2013), 14888, 1
- Sarin, N., Lasky, P. D., Sammut, L., & Ashton, G. 2018, *Phys. Rev. D*, 98, 043011
- Schulze, S., Levan, A. J., Malesani, D., et al. 2012, GRB Coordinates Network, Circular Service, No. 13257, #1 (2012), 13257, 1
- Selsing, J., Malesani, D., Kann, D. A., & Tanvir, N. R. 2018, GRB Coordinates Network, Circular Service, No. 22591, #1 (2018/April-0), 22591, 1
- Soderberg, A. M., Berger, E., & Ofek, E. 2005, GRB Coordinates Network, 4186, 1
- Tanvir, N. R., Wiersema, K., Levan, A. J., et al. 2012, GRB Coordinates Network, Circular Service, No. 13348, #1 (2012), 13348, 1
- Thoene, C. C., Levan, A., Jakobsson, P., et al. 2006, GRB Coordinates Network, 5373, 1
- Thompson, C. 1994, *MNRAS*, 270, 480
- Thompson, C., Lyutikov, M., & Kulkarni, S. R. 2002, *ApJ*, 574, 332
- Troja, E., Cusumano, G., O'Brien, P. T., et al. 2007, *ApJ*, 665, 599
- Turolla, R., Zane, S., & Watts, A. L. 2015, *Reports on Progress in Physics*, 78, 116901
- Usov, V. V. 1992, *Nature*, 357, 472
- Wiersema, K., Flores, H., D'Elia, V., et al. 2011, GRB Coordinates Network, Circular Service, No. 12431, #1 (2011), 12431, 1
- Woan, G., Pitkin, M. D., Haskell, B., Jones, D. I., & Lasky, P. D. 2018, *ApJ*, 863, L40
- Woosley, S. E. 1993, *ApJ*, 405, 273
- Xu, D., Fynbo, J. P. U., Malesani, D., et al. 2016, GRB Coordinates Network, Circular Service, No. 19109, #1 (2016), 19109, 1
- Xu, D., Heintz, K. E., Malesani, D., & Fynbo, J. P. U. 2017, GRB Coordinates Network, Circular Service, No. 20458, #1 (2017), 20458, 1
- Xu, D., Heintz, K. E., Malesani, D., Wiersema, K., & Fynbo, J. P. U. 2016, GRB Coordinates Network, Circular Service, No. 19773, #1 (2016), 19773, 1
- Xu, D., Malesani, D., Tanvir, N., Kruehler, T., & Fynbo, J. 2013, GRB Coordinates Network, Circular Service, No. 15450, #1 (2013), 15450, 1
- Yang, B., Jin, Z.-P., Li, X., et al. 2015, *Nature Communications*, 6, 7323
- Yu, Y.-W., Cheng, K. S., & Cao, X.-F. 2010, *ApJ*, 715, 477
- Zhang, B.-B., Liang, E.-W., & Zhang, B. 2007, *ApJ*, 666, 1002
- Zhang, B. 2011, *Comptes Rendus Physique*, 12, 206
- Zhang, B., Fan, Y. Z., Dyks, J., et al. 2006, *ApJ*, 642, 354
- Zhang, B., & Mészáros, P. 2001, *ApJ*, 552, L35
- Zou, L., Liang, E.-W., Lü, H.-J., et al. 2018, submitted

TABLE 1  
THE OBSERVATIONAL PROPERTIES AND FITTING RESULTS OF OUR SAMPLE.

GRB (Name)	$z$ Redshift	$T_{90}$ (second)	$L_0^a$ ( $10^{47}$ erg s $^{-1}$ )	$\tau^a$ ( $10^3$ s)	$n^b$	$\chi^2/\text{dof}^c$	References <sup>d</sup>
050319	3.24	153	$6.43 \pm 0.17$	$7.42 \pm 0.73$	$4.14 \pm 0.14$	1.27	(1)
050822	1.434	103	$0.447 \pm 0.01$	$13.27 \pm 1.14$	$4.45 \pm 0.11$	1.29	(2)
050922B	4.9	151	$0.74 \pm 0.04$	$198.43 \pm 53.14$	$2.94 \pm 0.26$	1.05	(3)
051016B	0.9364	4	$0.132 \pm 0.0004$	$13.89 \pm 1.53$	$3.8 \pm 0.13$	1.17	(4)
060604	2.68	80	$1.05 \pm 0.04$	$10.61 \pm 1.15$	$4.04 \pm 0.13$	1.32	(5)
060605	3.8	115	$11 \pm 0.27$	$8.91 \pm 0.78$	$2.48 \pm 0.08$	0.92	(6)
060714	2.71	115	$6.06 \pm 0.21$	$3.10 \pm 0.31$	$3.86 \pm 0.10$	1.27	(7)
060729	0.54	115	$0.175 \pm 0.0002$	$90.99 \pm 2.77$	$3.34 \pm 0.03$	1.25	(8)
061121	1.314	81	$14.6 \pm 0.18$	$2.79 \pm 0.09$	$3.71 \pm 0.03$	1.00	(9)
070129	2.3384	461	$0.705 \pm 0.02$	$20.45 \pm 1.90$	$3.95 \pm 0.12$	1.19	(10)
070306	1.496	209	$1.47 \pm 0.03$	$71.94 \pm 7.01$	$2.38 \pm 0.08$	1.42	(11)
070328	2.0627	75	$218 \pm 2.01$	$0.67 \pm 0.02$	$3.33 \pm 0.02$	1.35	(12)
070508	0.82	21	$32.5 \pm 0.25$	$0.61 \pm 0.01$	$3.56 \pm 0.02$	1.00	(13)
080430	0.767	14	$0.275 \pm 0.01$	$5.81 \pm 0.34$	$4.68 \pm 0.07$	1.00	(14)
081210	2.0631	146	$0.282 \pm 0.01$	$52.06 \pm 14.20$	$3.34 \pm 0.33$	1.11	(12)
090404	3.0	84	$2.03 \pm 0.05$	$19.77 \pm 1.82$	$3.63 \pm 0.11$	1.39	(15)
090516	4.109	208	$11.2 \pm 0.23$	$12.34 \pm 0.89$	$2.81 \pm 0.07$	1.08	(16)
090529	2.625	69	$0.105 \pm 0.01$	$49.45 \pm 23.12$	$4.03 \pm 0.62$	1.24	(17)
090618	0.54	113	$9.05 \pm 0.05$	$1.43 \pm 0.02$	$3.82 \pm 0.01$	1.17	(18)
091018	0.971	4	$13.5 \pm 0.28$	$0.32 \pm 0.02$	$4.12 \pm 0.04$	1.29	(19)
091029	2.752	39	$2.07 \pm 0.04$	$11.19 \pm 0.78$	$4.08 \pm 0.09$	1.09	(20)
100302A	4.813	18	$0.678 \pm 0.03$	$11.51 \pm 2.08$	$5.05 \pm 0.26$	0.80	(21)
100615A	1.398	39	$3.56 \pm 0.09$	$4.45 \pm 0.48$	$4.61 \pm 0.14$	1.01	(22)
100814A	1.44	175	$1.28 \pm 0.02$	$71.53 \pm 3.96$	$3.02 \pm 0.06$	1.78	(23)
110808A	1.348	48	$(7.42 \pm 0.46)\text{e-2}$	$13.46 \pm 3.89$	$4.87 \pm 0.41$	1.08	(24)
111008A	4.9898	63	$25.8 \pm 0.54$	$6.46 \pm 0.42$	$3.69 \pm 0.07$	1.11	(25)
111228A	0.714	101	$0.751 \pm 0.01$	$6.79 \pm 0.37$	$3.97 \pm 0.06$	1.01	(26)
120422A	0.283	7	$(6.39 \pm 0.46)\text{e-4}$	$165.35 \pm 77.30$	$3.63 \pm 0.66$	1.12	(27)
120521C	6.0	27	$1.88 \pm 0.13$	$11.83 \pm 6.19$	$3.12 \pm 0.64$	1.08	(28)
130609B	1.3	211	$26.5 \pm 0.32$	$4.03 \pm 0.17$	$2.72 \pm 0.04$	1.00	(29)
131105A	1.686	112	$2.25 \pm 0.07$	$4.01 \pm 0.59$	$4.02 \pm 0.17$	1.13	(30)
140430A	1.6	174	$0.563 \pm 0.02$	$5.59 \pm 1.35$	$4.87 \pm 0.41$	1.17	(31)
140703A	3.14	70	$20.9 \pm 0.57$	$20.13 \pm 2.05$	$2.17 \pm 0.08$	1.19	(32)
160227A	2.38	317	$3.04 \pm 0.08$	$23.52 \pm 1.99$	$3.77 \pm 0.10$	1.49	(33)
160804A	0.736	144	$0.118 \pm 0.0004$	$6.32 \pm 0.99$	$5.26 \pm 0.26$	1.08	(34)
161117A	1.549	126	$3.84 \pm 0.08$	$4.15 \pm 0.26$	$4.18 \pm 0.08$	1.12	(35)
170113A	1.968	21	$16.4 \pm 0.32$	$1.56 \pm 0.10$	$4.17 \pm 0.07$	1.24	(36)
170519A	0.8181	216	$0.524 \pm 0.01$	$11.70 \pm 1.20$	$2.99 \pm 0.12$	1.24	(37)
170531B	2.366	164	$0.952 \pm 0.07$	$4.88 \pm 1.61$	$4.01 \pm 0.49$	1.20	(38)
170607A	0.557	320	$0.187 \pm 0.0004$	$16.20 \pm 1.26$	$4.43 \pm 0.11$	1.45	(39)
170705A	2.01	207	$6.15 \pm 0.13$	$9.47 \pm 0.59$	$4.28 \pm 0.08$	1.77	(40)
171222A	2.409	175	$0.114 \pm 0.01$	$126.70 \pm 71.35$	$4.01 \pm 0.91$	1.36	(41)
180325A	2.25	94	$114 \pm 2.23$	$2.99 \pm 0.20$	$2.54 \pm 0.05$	1.01	(42)
180329B	1.998	210	$2.57 \pm 0.08$	$8.17 \pm 1.16$	$3.04 \pm 0.17$	1.30	(43)
180404A	1.0	701	$0.182 \pm 0.01$	$7.73 \pm 3.11$	$4.1 \pm 0.42$	1.02	(44)

REFERENCES. — (1)Fynbo et al. 2005;(2)Hjorth et al. 2012;(3)Perley et al. 2016;(4)Soderberg et al. 2005;(5)Castro-Tirado et al. 2006;(6)Peterson & Schmidt 2006;(7)Jakobsson et al. 2006;(8)Thoene et al. 2006;(9)Bloom et al. 2006;(10)Kruehler et al. 2012;(11)Jaunsen et al. 2007;(12)Kruehler et al. 2015;(13)Jakobsson et al. 2007;(14)Cucchiara & Fox. 2008;(15)Perley et al. 2013;(16)de Ugarte Postigo et al. 2009;(17)Malesani et al. 2009;(18)Cenko et al. 2009;(19)Chen et al. 2009;(20)Chornock et al. 2009;(21)Chornock et al. 2010;(22)Kruehler et al. 2013;(23)O’Meara et al. 2010;(24)de Ugarte Postigo et al. 2011;(25)Wiersema et al. 2011;(26)Dittmann et al. 2011;(27)Schulze et al. 2012;(28)Tanvir et al. 2012;(29)Ruffini et al. 2013;(30)Xu et al. 2013;(31)Kruehler et al. 2014;(32)Castro-Tirado et al. 2014;(33)Xu et al. 2016a;(34)Xu et al. 2016b;(35)Malesani et al. 2016;(36)Xu et al. 2017;(37)GCN 21119;(38)GCN 21177;(39)GCN 21240;(40)de Ugarte Postigo et al. 2017a;(41)de Ugarte Postigo et al. 2017b;(42)Heintz et al. 2018;(43)Izzo et al. 2018;(44)Selsing et al. 2018

<sup>a</sup> The plateau luminosity and break time of the X-ray light curves in our sample.

<sup>b</sup> The derived braking index of magnetar.

<sup>c</sup> The goodness of the X-ray light-curve fitting using the magnetar model and power-law component if possible.

<sup>d</sup> The references for the redshift in our sample.

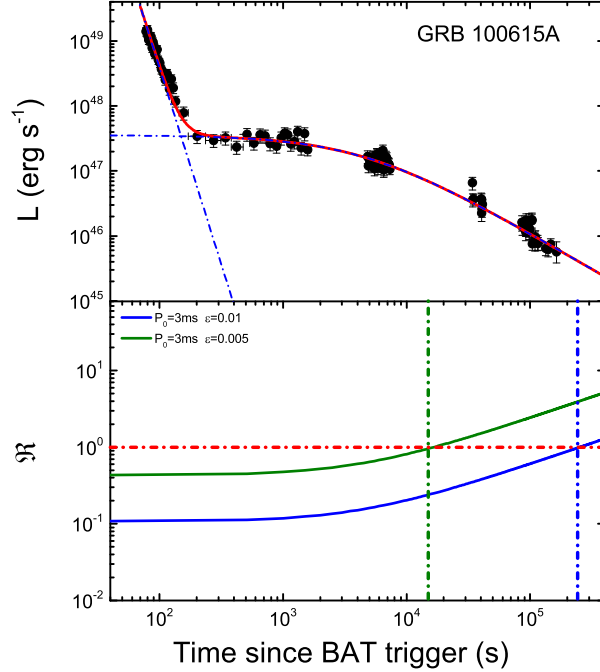


FIG. 1.— An example light-curve fitting for GRB 100615A. Upper panel: the X-ray light curves with power-law and magnetar models fits (blue dashed-dotted lines). The red solid line is the superposition of power-law and magnetar models. Lower panel: the ratio between the EM luminosity and GW luminosity as a function of time with  $\varepsilon = 0.01$  (blue solid line) and  $\varepsilon = 0.005$  (olive solid line) by assuming  $P_0 = 3$  ms.

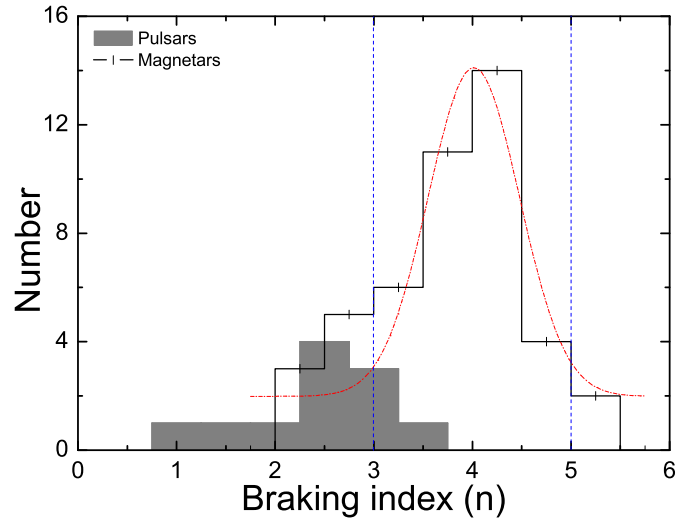


FIG. 2.— Distribution of braking index (solid black line) and the best-fit Gaussian profile (red dashed line). The gray filled histogram is the braking index of all known pulsar where the long-term spindown is believed to be electromagnetically dominated. The two vertical dotted lines are corresponding to  $n = 3$  and  $n = 5$ , respectively.

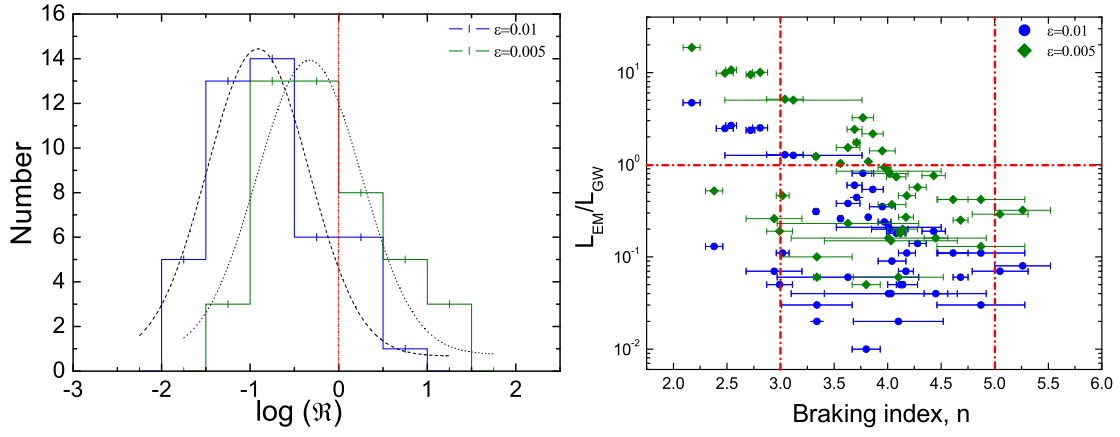


FIG. 3.— Left: distributions of  $\mathfrak{R}$  and its best-fit Gaussian profile for  $\epsilon = 0.01$  (blue solid line) and  $\epsilon = 0.005$  (olive solid line). Right: derived the ration between luminosity of EM and GW radiation as function of braking index with  $\epsilon = 0.01$  (black solid points) and  $\epsilon = 0.005$  (blue solid diamond). The horizontal dash-dotted line is  $\mathfrak{R} = 1$ , and two vertical dash-dotted lines are  $n = 3$  and  $n = 5$ , respectively.